JACC Vol. 29, No. 5
April 1997:1081–8





# Interactions Between Microbubbles and Ultrasound: In Vitro and In Vivo Observations

KEVIN WEI, MD, DANNY M. SKYBA, PHD, CHRISTIAN FIRSCHKE, MD,
ANANDA R. JAYAWEERA, PHD, JONATHAN R. LINDNER, MD, SANJIV KAUL, MD, FACC

*Charlottesville, Virginia*

***Objectives.*** **We attempted to examine the interactions between ultrasound and microbubbles.**

***Background.*** **The interactions between microbubbles and ultrasound are poorly understood. We hypothesized that 1) ultrasound destroys microbubbles, and 2) this destruction can be minimized by limiting the exposure of microbubbles to ultrasound.**

***Methods.*** **We performed in vitro and in vivo experiments in which microbubbles were insonated at different frequencies, transmission powers and pulsing intervals. Video intensity decay was measured in vitro and confirmed by measurements of microbubble size and concentrations. Peak video intensity and mean microbubble myocardial transit rates were measured in vivo.**

***Results.*** **Imaging at lower frequencies and higher transmission powers resulted in more rapid video intensity decay ($p = 0.01$), and decreasing exposure of microbubbles to ultrasound minimized their destruction in vitro. Although these effects were also noted in vivo with venous injections of microbubbles, they were not seen with aortic root or direct coronary artery injections.**

***Conclusions.*** **Ultrasound results in microbubble destruction that is more evident at lower frequencies and higher acoustic powers. Reducing the exposure of microbubbles to ultrasound minimizes their destruction. This effect is most marked in vivo with venous rather than aortic or direct coronary injections of microbubbles. These findings could lead to effective strategies for myocardial perfusion imaging with venous injections of microbubbles.**

*(J Am Coll Cardiol 1997;29:1081–8)*


Assessment of myocardial perfusion from a venous injection of microbubbles is now feasible with the development of two advances in ultrasound imaging. The first is intermittent imaging (1). After venous injection of microbubbles, a transient but significant increase in myocardial opacification occurs during the initial exposure to ultrasound after its transmission is suspended for a short period (1). The second advance is harmonic imaging (2). Acoustic signals emanating from microbubbles are much more likely to contain harmonics than are those returning from tissue (2–4). Thus, transmitting ultrasound at one frequency but receiving a harmonic of that frequency results in a decrease in clutter and an increase in the signal to noise ratio during contrast echocardiography (2). The combination of intermittent and harmonic imaging results in excellent myocardial opacification during venous injection of microbubbles (1). However, the mechanisms underlying the success of intermittent harmonic imaging are poorly understood. We hypothesized that 1) ultrasound destroys microbubbles, and 2) decreasing the exposure of microbubbles to ultrasound results in less bubble destruction and better myocardial opacification. We tested these hypotheses using in vitro and in vivo experiments.

## Methods

**In vitro experiments.** Two ultrasound contrast agents, Albunex and FS-069 (Molecular Biosystems Inc.), were used in these experiments. These agents consist of air-filled and perfluoropropane-filled albumin microspheres, respectively, and have a mean size of 4.3 and 3.9 $\mu$m and a mean concentration of $5 \times 10^8 \cdot ml^{-1}$ and $8 \times 10^8 \cdot ml^{-1}$, respectively (5). Variable doses of these agents were mixed with 4 liters of 0.9% saline solution in a glass beaker. A magnetic stirrer ensured constant mixing of the bubbles. The transducer was held in a fixed position in the center of the beaker, 2 cm into the solution, at a location where artifacts from the edges of the beaker and the stirrer were minimal. The bubble solutions were exposed to different frequencies, transmission powers

From the Cardiovascular Division, University of Virginia, Charlottesville, Virginia. This work was supported in part by Grant R01-HL48890 from the National Institutes of Health, Bethesda, Maryland to Dr. Kaul and a grant-in-aid from the Virginia Affiliate of the American Heart Association, Glen Allen, Virginia to Dr. Jayaweera. It was also supported by a grant from Molecular Biosystems, Inc., San Diego, California and by equipment grants from Hewlett-Packard Corporation, Andover, Massachusetts and ATL-Interspec, Bothell, Washington. Dr. Wei is the recipient of a Junior Personnel Research Fellowship from the Heart and Stroke Foundation of Canada, Ottawa, Canada, and Dr. Skyba is the recipient of Postdoctoral Fellowship Grant F32-HL09540 from the National Institutes of Health, Bethesda, Maryland. Dr. Firschke was the recipient of a grant from Deutsche Gesellschaft fuer Ultraschall in der Medizin, Stuttgart, Germany, and Dr. Lindner was the recipient of a Fellowship Training Grant from the Virginia affiliate of the American Heart Association. Dr. Kaul is an Established Investigator of the National Center of the American Heart Association, Dallas, Texas.

Manuscript received August 27, 1996; revised manuscript received December 19, 1996, accepted January 9, 1997.

Address for correspondence: Dr. Sanjiv Kaul, Cardiovascular Division, Box 158, University of Virginia Medical Center, Charlottesville, Virginia 22908. E-mail: sk@virginia.edu.


Published by Elsevier Science Inc.

0735-1097/97/$17.00
PII S0735-1097(97)00029-6

and durations of exposure to ultrasound. Ultrasound-exposed and nonexposed solutions were examined with an Electrozone Celloscope (model 112 LTH, Particle Data) to determine the size and concentration of microbubbles (6).

**In vivo experiments.** The study protocol was approved by the Animal Research Committee at the University of Virginia and conformed to the American Heart Association Guidelines for Use of Animals in Research. Eight anesthetized open chest adult mongrel dogs were studied. In seven dogs, Albunex was injected through a 7F catheter placed in the aortic root with a prototype low volume, high accuracy power injector (Medrad). A dose of 1.5 to 5 ml of Albunex that resulted in optimal myocardial opacification in individual dogs was chosen and then held constant for the duration of the study. A 3-ml saline flush was used and the total volume was injected over 3 s. In the same dogs, 1 ml of FS-069 was also injected through a 7F catheter in the right atrium followed by a 5-ml saline flush over 1.5 s.

In one dog, the proximal left anterior descending coronary artery was ligated and perfused through a cannula with arterial blood diverted from the right carotid artery. Flow to the cannula was controlled with a peristaltic pump (model 2501, Harvard Apparatus) and was measured with an extracorporeal time of flight ultrasound flow probe (model SC, Transonics) (7). Flow rates were adjusted from 15 to 60 $ml \cdot min^{-1}$ in random order. Four injections of Albunex (1 ml over 1 s) were performed at every flow rate to allow both continuous and intermittent imaging at two mean frequencies (4 and 6 MHz).

**Contrast echocardiography.** For all in vitro and in vivo experiments (except those involving direct coronary artery injections of microbubbles), imaging was performed with the use of a prototype phased-array system (Hewlett-Packard) capable of continuous and intermittent imaging in both fundamental and harmonic modes. A different system (HDI-3000, ATL-Interspec) was used for the experiment involving direct coronary injections of microbubbles. Although this system is also capable of both fundamental and intermittent imaging, only the fundamental mode was used during both continuous and intermittent imaging. For both systems, ultrasound is transmitted and received along a specific line within a 90° sector every 33 ms during continuous imaging. With intermittent imaging, a sector is formed at discrete time intervals with the use of either an internal timer or electrocardiographic gating. In the latter instance, no ultrasound is transmitted except during the 33 ms required to create the 90° sector at the discrete time specified.

For most experiments, a transducer that transmits at a mean frequency of 2 MHz was used. During fundamental imaging, the same frequency is received; during harmonic imaging, a multiple of this frequency (in this case 4 MHz) is received. To study the effect of frequency on microbubble destruction, transducers with mean transmission frequencies of 2.7, 5.5 and 7.5 MHz were also used for the in vitro experiments. For the experiment involving direct intracoronary injections of microbubbles, 4- and 6-MHz transducers were used. All experiments were performed with the same logarithmic compression to allow comparison of video intensity between stages. The gain settings were optimized for each form of imaging at the beginning of the experiment and then held constant throughout. Because signals returning from tissue are weaker during harmonic than during fundamental imaging, the receive gain was increased during harmonic imaging to produce images obtained before injection of contrast medium that had the same myocardial video intensity as those obtained during fundamental imaging. Data were recorded on 1.25-cm videotape by using an S-VHS recorder (Panasonic model AG6200, Matsushita Electrical Co.) for later analysis.

Images were digitized as previously described (7). For the in vitro experiments, a large region of interest (≥3,000 pixels) was defined around the focal point of the transducer, with care taken to avoid the edges of the beaker. The background-subtracted video intensity from this region was then plotted against time and fitted to a sigmoid function:

$$y = A\frac{\exp[-\lambda(t - t_s)]}{1 + \exp[-\lambda(t - t_s)]} + C,$$

where y is video intensity; A is peak intensity, t is time, $t_s$ is the time at which maximal slope occurs, $\lambda$ is the maximal slope denoting the rate of video intensity decay and C is the background video intensity (8). Although our data were background subtracted, the constant C was still used to minimize any errors in calculation of background. All the decay curves analyzed could be fitted well to the sigmoid function, with a correlation coefficient of $r > 0.90$.

For the in vivo experiments, consecutive end-systolic frames, which included the period from just before contrast injection until 10 s thereafter, were selected and aligned by using computer cross correlation (9). A large transmural region of interest was defined over the anterior myocardium, and the average video intensity within the region was determined for all end-systolic frames. The video intensity from several frames before the appearance of contrast medium in the myocardium was considered to represent background. Time-intensity plots were generated from the background-subtracted video intensity data and a gamma variate function, $y = Ate^{-\alpha t}$, was applied to them, where A is a scaling factor, t is time and $\alpha$ is proportional to the transit rate of the tracer (9).

**Statistical methods.** Comparisons were performed by using a Student *t* test. The Bonferroni correction was implemented for comparison of more than two sets of values. Correlations were performed by using linear regression analysis. Differences were considered significant at $p < 0.05$ (two-sided).

## Results

**In vitro experiments.** *Effect of transmission frequency.* The 5.5- and 7.5-MHz frequencies were from the same transducer which was calibrated to produce similar pressure profiles during transmission of both frequencies. The transmission power for all transducers (including the 2.7-MHz transducer)

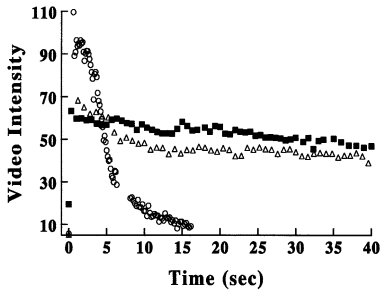


**Figure 1.** Time-intensity curves obtained for Albunex during continuous fundamental imaging using transducers with three separate frequencies—2.7 MHz (**open circles**), 5.5 MHz (**solid squares**) and 7.5 MHz (**open triangles**)—adjusted to generate similar transmission powers. The dose of Albunex used was similar at the three frequencies.

was adjusted to be similar. At these settings, the peak negative acoustic pressures were calculated to be 0.7 MPa for the 5.5- and 7.5-MHz transducers and 1.0 MPa for the 2.7-MHz transducer. The dose of Albunex was held constant for all injections. Time-intensity curves obtained for Albunex during continuous fundamental imaging with the three different transducer frequencies are depicted in Figure 1. The peak video intensity was significantly higher ($p < 0.01$) at the 2.7-MHz frequency than at the higher frequencies. It also decreased at a dramatically higher rate ($p = 0.01$) at this frequency ($\lambda = 0.81$) than at the higher frequencies, which showed similar decay rates ($\lambda = 0.09$ and $\lambda = 0.04$, respectively, at 5.5 and 7.5 MHz, $p = 0.10$).

*Effect of harmonic versus fundamental imaging.* Figure 2A illustrates the effects of fundamental versus harmonic imaging on video intensity decay of FS-069. Although the transmission frequency (2 MHz) was identical for both forms of imaging, the ultrasound energy delivered during harmonic imaging was higher because the pulse length was almost double that used for fundamental imaging. It can be seen that the peak video intensity generated during harmonic imaging was significantly greater than that generated during fundamental imaging ($71 \pm 0.4$ vs. $22 \pm 2.2$ gray scale units, respectively, $p = 0.001$). The video intensity decay was also faster during harmonic than during fundamental imaging ($\lambda = 0.28$ vs. 0.15, $p < 0.01$).

*Effect of imaging rate.* Figure 2B illustrates the effect of the imaging rate on the decay of FS-069 with harmonic imaging, which was performed with a 2-MHz transducer and a pulsing interval of 250 ms. In the first curve an initial increase in the video intensity occurs as the bubbles mix with saline solution, which is followed by a gradual decay. The experiment was then repeated with the same dose of microbubbles and imaging variables. This time, ultrasound transmission was interrupted for 30 s, 45 s after the introduction of microbubbles. It can be seen from the second curve that when imaging was resumed, the video intensity was unchanged. The results of a similar experiment executed with Albunex are shown in Figure 3A. Again, no change in the video intensity was seen after imaging was restarted after two separate pauses. At the same system settings and pulsing interval of 500 ms, the rate of video

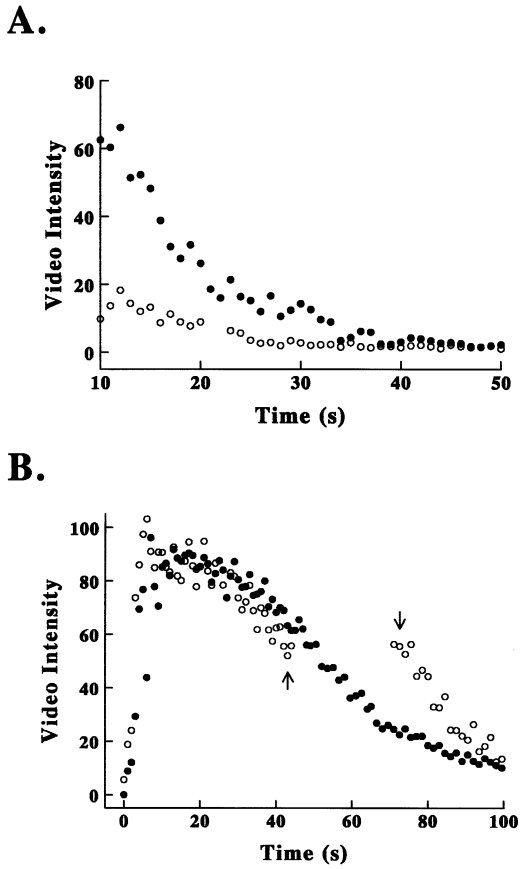


**Figure 2. A,** Effect of fundamental (**open circles**) and harmonic (**solid circles**) imaging on video intensity decay of FS-069 during continuous transmission of ultrasound using the same transmission frequency (2 MHz). **B,** Effect of no pause (**solid circles**) and a 30-s pause (**open circles, arrows**) in ultrasound transmission on video intensity decay of FS-069.

intensity decay was greater for Albunex than for FS-069 ($\lambda = 0.75$ vs. 0.08, $p < 0.01$). These experiments were also performed with FS-069 and Albunex in degassed saline solution (Fig. 3B). The decays of the time-intensity plots from FS-069 were similar between the aerated and degassed solutions ($\lambda = 0.08$ and 0.11, respectively, $p = NS$). The decay occurred so rapidly for Albunex in degassed saline solution that a time-intensity curve could not be obtained.

To further examine the effect of imaging rate on video intensity decay, time-intensity plots for the same dose of FS-069 were generated at different pulsing intervals during fundamental imaging with the use of a 2-MHz transducer. As the pulsing interval was increased from 33 to 1,000 ms, greater persistence of the contrast effect was seen (Fig. 4A). Figure 4B illustrates the relation between the pulsing interval and video intensity measured at 30 s from the curves shown in Figure 4A. As the pulsing interval increased, the video intensity at 30 s also increased until the pulsing interval reached 450 ms, beyond which video intensity at 30 s reached a plateau.

Solutions of FS-069 were exposed to continuous and intermittent fundamental imaging (an image formed every 500 ms

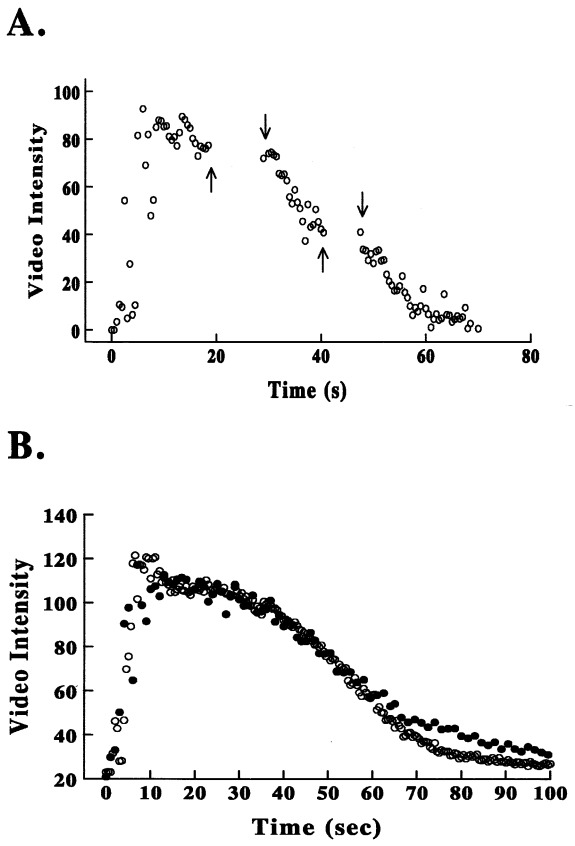


**Figure 3.** Time-intensity plots with intermittent harmonic imaging (pulsing interval 250 ms) with **(A)** Albunex with two pauses **(arrows)** in ultrasound transmission and **(B),** FS-069 microbubbles in aerated **(solid circles)** and degassed **(open circles)** saline solution.

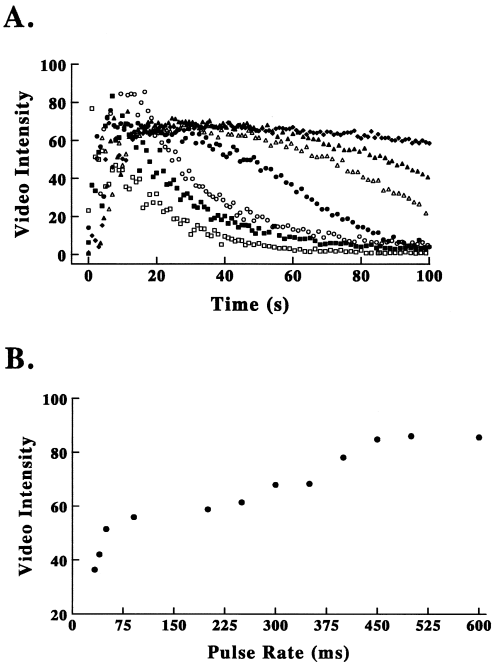


**Figure 4. A,** Effect of imaging rate on the persistence of FS-069. **Open squares** = 33 ms; **solid squares** = 50 ms; **open circles** = 83 ms; **solid circles** = 250 ms; **open triangles** = 375 ms; **solid triangles** = 500 ms; **solid diamonds** = 1,000 ms. **B,** Video intensity data from **panel A** after 30-s exposure to separate intermittent imaging sequences (33-ms to 600-ms pulse intervals) plotted against the pulsing interval.

in the latter case) for 30 s, and samples were then examined with a particle counter to determine the concentration and size of the microbubbles. The concentrations of microbubbles in solutions subject to no ultrasound exposure, intermittent imaging and continuous imaging were $2.94 \times 10^5 \cdot \mu l^{-1}$, $2.76 \times 10^5 \cdot \mu l^{-1}$ and $1.71 \times 10^5 \cdot \mu l^{-1}$, respectively. The average microbubble size measured with the Electrozone Celloscope during no ultrasound exposure and intermittent imaging at 500 ms was 2.4 $\mu$m, whereas that during continuous imaging was 0.8 $\mu$m.

*Effect of transmission power.* The effect of transmission power (using a 2-MHz transducer) on the microbubble backscatter of FS-069 during intermittent fundamental and harmonic imaging is shown in Figure 5A. A setting of 50% of the maximal transmission power resulted in a greater video intensity decay than that seen at a setting of 25% of the maximal power ($\lambda$ = 0.7 vs. 0.18 for fundamental, and 1.31 vs. 0.67 for harmonic imaging, respectively, p = 0.01). Figure 5B illustrates results of a similar experiment performed by using continuous imaging with a 5.5-MHz transducer. Video intensity decay is more rapid at the higher power settings. However, these transducers are not comparable in total acoustic power.

**In vivo experiments.** *Venous injection of contrast medium.* Venous injections of FS-069 resulted in much wider myocardial time-intensity profiles than those seen with aortic root or direct coronary injections of Albunex because of the wider input function caused by bolus dispersion in the lungs in the former (5). Intermittent imaging resulted in greater peak background-subtracted myocardial video intensity than did continuous imaging, for both fundamental (26 ± 31 vs. 8 ± 5 U, $p < 0.001$) and harmonic (56 ± 22 vs. 11 ± 9 U, $p < 0.001$) imaging. The combination of intermittent and harmonic imaging resulted in the greatest ($p < 0.05$) myocardial opacification compared to all other forms of imaging.

*Aortic root injection of contrast medium.* The myocardial peak video intensity for the seven dogs was 23 ± 7 and 30 ± 9 U for continuous and intermittent fundamental imaging (p = 0.21), and 62 ± 19 and 45 ± 17 U for continuous and intermittent harmonic imaging (p = 0.07), respectively. Thus, although it was higher during harmonic than during fundamental imaging, the rate of acquisition (intermittent vs. continuous) did not influence the myocardial peak video intensity measurement in either mode of imaging. The mean myocardial microbubble transit rates for the seven dogs were also not significantly different and measured, respectively, 1.11 ± 0.23 and 1.06 ± 0.2 $s^{-1}$ for continuous and intermittent fundamental imaging (p = 0.74) and 1.26 ± 0.25 and 1.33 ± 0.42 $s^{-1}$ for continuous and intermittent harmonic imaging (p = 0.72).

*Direct coronary artery injection of contrast medium.* In the single dog in which Albunex was injected directly into the

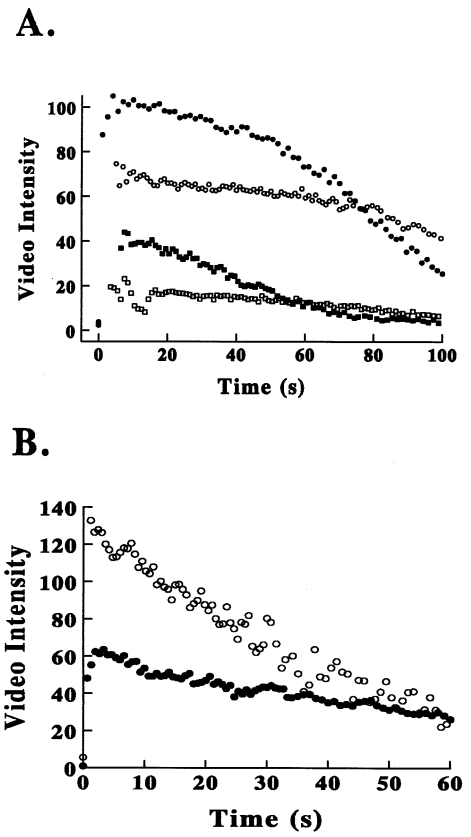


**Figure 5.** Effect of transmission power on the rate of video intensity decay of FS-069 during fundamental imaging with 2.0-MHz (**A**) and 5.5-MHz (**B**) transducers. The former is during the intermittent and the latter during the continuous mode. PP = peak pressure as a function of transmission power. **A, Solid** and **open circles** = harmonic PP of 650 and 463 kPa, respectively; **solid** and **open squares** = fundamental PP of 650 and 463 kPa, respectively. **B, Solid** and **open circles** = PP of 75 and 300 W/cm$^2$, respectively.

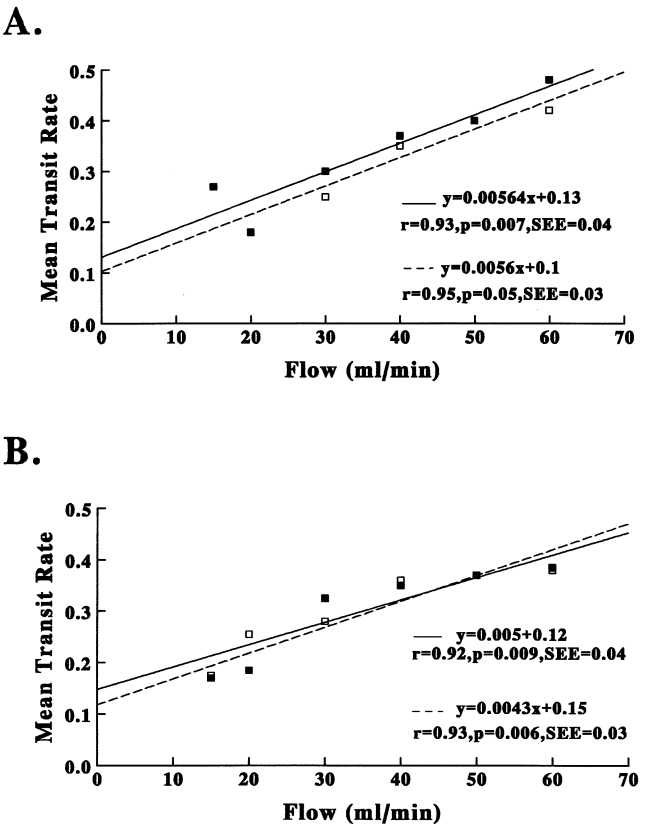


**Figure 6.** Plots of mean myocardial transit rate of microbubbles versus coronary blood flow when fundamental imaging was performed with a 4-MHz (**A**) and a 6-MHz (**B**) transducer and Albunex was injected directly into the coronary artery as an instantaneous bolus in a single dog. The relation during continuous imaging is depicted as a **solid line,** that during intermittent imaging as a **dashed line.**

coronary artery, the imaging rate had no effect on the time-intensity plots obtained at the same coronary flow rate. The peak video intensity for the 4-MHz transducer was, respectively, 30 ± 6 and 33 ± 6 U (p = 0.20) for intermittent and continuous imaging and 43 ± 13 and 42 ± 10 U (p = 0.80) for the 6-MHz transducer. Figure 6 shows the relation between mean myocardial microbubble transit rates obtained from a direct coronary injection of Albunex, and flow probe determinations of coronary blood flow during continuous and intermittent imaging. No significant differences were noted between the correlations for the two transducers during continuous and intermittent imaging.

## Discussion

**Why does intermittent imaging produce a greater contrast effect?** During the initial exposure to ultrasound after imaging was suspended for a short period, Porter and Xie (1) observed a transient but significant increase in myocardial opacification with venous injection of microbubbles. They attributed this finding to a transient increase in backscatter produced by a direct effect of ultrasound and used the term "transient response imaging" to define the phenomenon. There are three possible ways in which ultrasound could increase backscatter: 1) acoustic cavitation, in which new gas bubbles are forced out of solution by the acoustic power of ultrasound; 2) a transient enlargement of bubbles already present in the field on exposure to ultrasound; and 3) an increase in bubble size caused by back-diffusion of gases during the suspension of ultrasound transmission.

The pressure required for acoustic cavitation in water can be achieved by instruments in clinical use (10) and has been demonstrated experimentally (11). It has also been shown that bubbles can enlarge when exposed to an ultrasound field (12). However, both effects are transient, lasting for only milliseconds (11). Growth in bubble size by back-diffusion of gases that are at higher partial pressures in the medium than in the bubbles has also been reported (13).

In our in vitro experiments, microbubbles were suspended in a glass beaker with a magnetic stirrer so that they were constantly entering and leaving the ultrasound beam. Therefore, the video intensity at any point in time within the region

of interest represented the average video intensity in the entire beaker and not just that within the ultrasound beam itself. In this system, with no bubble flux, an increase in video intensity was not observed after a pause in the transmission of ultrasound. The absence of any increase in the video intensity after resumption of ultrasound transmission suggests that either the three effects just described were not operational or that they were too brief to cause any change in measured backscatter.

Even though transient cavitation is an unlikely mechanism for the increased video intensity, it is possible that microcavitation undetectable by our ultrasound systems contributes to bubble destruction. Explosion of small microbubbles caused by cavitation can conceivably destroy neighboring bubbles. Because microcavitation requires that gas be present in the medium, we compared the video intensity decay rates of microbubbles by using both aerated and degassed saline solution, and we found similar decay in both solutions. Therefore, our results do not support the role of microcavitation for either a transient increase in video intensity or for microbubble destruction.

Our experiments provide both direct and indirect evidence that ultrasound destroys microbubbles. The decay in video intensity during ultrasound exposure, and the lack of this decay with cessation of ultrasound transmission, provides indirect evidence for this effect. Direct evidence of microbubble destruction comes from our measurements of microbubble size and concentration before and after exposure to ultrasound. Like others (7), we found that a sigmoid function best describes microbubble decay in solutions. Each curve is characterized by an initial flat slope, which indicates that bubbles closest to the transducer shield other bubbles from destruction, since a concentrated bubble solution impedes the transmission of ultrasound (13). As bubbles are destroyed, there is less shielding, resulting in accelerated bubble destruction, which is represented by the steep portion of the curve. The second flattening of the curve is probably caused by the smaller bubbles that are not destroyed or are created by the disintegration of larger bubbles during ultrasound exposure.

In comparison with the in vitro observations, and similar to Porter and Xie (1), we noted a dramatic but transient increase in myocardial opacification after a pause of ultrasound transmission during venous injection of microbubbles in dogs. The difference between the in vitro and in vivo settings is that the former represents a closed system, whereas the latter does not. During the pause in ultrasound transmission, microbubbles in the pulmonary circulation and left ventricular cavity that have not been destroyed by ultrasound enter the coronary microcirculation. Interrupting ultrasound transmission results in greater opacification by permitting the myocardial sample being insonated to become replenished with these bubbles.

The elevation (thickness) of an ultrasound beam is ~0.5 cm. Microbubbles that exhibit a microvascular rheology similar to that of red blood cells (7,15) have a mean velocity in tissue of ~0.1 to ~0.2 $cm \cdot s^{-1}$ at baseline. It will therefore take 3 to 5 s in the absence of ultrasound to completely fill the elevation with new microbubbles. Thus, the best contrast effect will be noted with a long pulsing interval. If imaging is performed at a rate faster than the rate of microbubble replenishment, microbubbles will be continuously destroyed and no tissue perfusion will be seen. However, if the velocity of microbubbles is greater than the pulsing interval, contrast effect will be noted. This is the reason why larger vessels (such as septal perforators, where the velocity of red blood cells is an order of magnitude higher than that in the microvessels) are seen even during continuous harmonic imaging, whereas no perfusion is noted in the microvasculature (16).

Why, then, is this effect of intermittent imaging not noted during aortic root or direct coronary injections of microbubbles? Myocardial concentrations of microbubbles are much higher after aortic or coronary than after venous injections, so that destruction of a portion of the microbubbles may not result in an appreciable change in video intensity. Furthermore, the use of higher frequencies results in less bubble destruction even during continuous imaging. These results have important bearing on our previous data (7,17) showing a close correlation between mean microbubble transit rate and myocardial blood flow with direct coronary injections of microbubbles. Therefore, as long as microbubbles are not destroyed in appreciable quantities, the use of tracer kinetic principles remains valid for the measurement of mean transit rates through tissues during arterial injections of microbubbles.

**Why does ultrasound destroy microbubbles?** Although our results indicate that ultrasound destroys microbubbles, the exact mechanism causing this effect is not addressed by our experiments. It is possible that either the induction of nonlinear oscillations or a direct physical impact of ultrasound, or a combination of both, results in bubble destruction. Because of their compressibility, bubbles in an ultrasound field undergo radial oscillations that are maximal at the resonating frequency (2,3,18). The bubbles that cause myocardial opacification from a venous injection have a diameter of ~4 to 6 $\mu$m. The resonant frequencies of bubbles this size are, by serendipity, in the range of frequencies used clinically in adults. Smaller bubbles have resonant frequencies that are above the clinically useful range in most adults, whereas larger bubbles cannot cross the pulmonary microcirculation.

On the basis of our results, it is attractive to postulate that nonlinear oscillations produced at the resonant frequency cause microbubble destruction. The higher rate of destruction at the 2.7-MHz frequency than at the higher frequencies (Fig 1A) would support this contention as the resonant frequency of Albunex is in this range (19). Given its similar size and shell structure, FS-069 would also be expected to have the same resonant frequency. Because harmonic signals can emanate from microbubbles during resonance (2,3,13), it is possible that the bubbles oscillate nonlinearly, release harmonic signals (7,15) and are then destroyed. The success of intermittent harmonic imaging could almost entirely be attributed to this cascade of events.

The acoustic power to which a microbubble is exposed, however, is related not only directly to the transmission power but also inversely to the square root of the transmission

frequency. Thus, although we could keep the transmission power the same during all frequencies, we could not control for the total acoustic power. As stated, the peak negative acoustic pressure is greater for a lower frequency transducer, and thus the total acoustic power is higher. We also noted greater microbubble decay during harmonic than during fundamental imaging when using a 2-MHz transducer. If resonance were the primary cause for bubble destruction, this phenomenon would not occur because the transmission frequency used for both forms of imaging is the same. We also noted that the increase in myocardial opacification was greater when ultrasound was paused during harmonic compared with fundamental imaging. In the instrument we used, the ultrasound energy delivered is higher per image line during harmonic than during fundamental imaging because the ultrasound pulse is almost twice as long during the former, which can explain these observations.

Increase in acoustic power may explain bubble destruction, a view that is also supported by the finding that increasing the transmission power enhances bubble destruction at any frequency. Similar results have been previously reported (20). Even though others (8,21) have shown that the ambient pressure also affects bubble integrity, the peak negative pressure of ultrasound far exceeds peak left ventricular systolic pressures. The peak pressures around the focal point of the 2-MHz transducer used in our study was 463 kPa ($3.5 \times 10^3$ mm Hg) at a power setting of 25% of maximal and 650 kPa ($4.9 \times 10^3$ mm Hg) at a setting of 50% of maximal.

On the basis of the preceding discussion, it is conceivable that ultrasound can directly cause bubble destruction without first causing resonance. Why, then, is myocardial opacification better at the resonant frequency? The acoustic emission caused by bubble destruction contains many frequencies, including the harmonic frequency. Thus, it is not necessary to invoke nonlinear oscillations as the sole mechanism for increased opacification during harmonic imaging. Irrespective of the mechanism underlying the production of harmonic signals from microbubbles, because tissue has few harmonic properties (22), the signal to noise ratio after microbubble injection is significantly greater during harmonic than during fundamental imaging (where the signal includes backscatter from both bubbles and tissue), resulting in better myocardial opacification. Therefore, greater destruction of microbubbles can explain both the faster rate of video intensity decay and the higher video intensity during intermittent imaging when the harmonic rather than the fundamental mode is used.

**Unique properties of different microbubbles.** Our results pertain to only two commercially produced microbubbles. The interaction with ultrasound may be different for other agents. Even in our experiments, the rate of video intensity decay of FS-069 was noted to be slower than that of Albunex, although both microbubbles have the same shell (5). It is possible that even if the shell of the FS-069 microbubble were destroyed by ultrasound as easily as that of Albunex, the low solubility of perfluoropropane could allow the gases to remain in suspension longer than the highly soluble air present in Albunex. Products similar to Albunex, but with a thicker shell, may not be physically destroyed by ultrasound, although ultrasound at high acoustic pressure might force air out of the shells, producing harmonic signals before they dissolve in blood. Having lost their gas content, these bubbles may not produce enough signals on subsequent ultrasound exposure.

Depending on their shell composition or method of preparation, some microbubbles may not be destroyed by ultrasound. In light of the preceding discussion, these bubbles would be unlikely to exhibit increased signals during harmonic imaging. Other microbubbles, because their small size makes them inefficient scatterers of ultrasound, may depend entirely on bubble destruction for their acoustic effects (23). Several of the microbubbles studied by us (24–26) seem to have properties that are qualitatively similar to those of FS-069 described here.

Bubble destruction by ultrasound may have other interesting applications. For instance, destroying microbubbles within the ultrasound beam and measuring their reappearance rate might allow quantification of the mean myocardial microbubble velocity during continuous venous infusions (26). Similarly, using a long pulsing interval to allow microbubble saturation of the beam could permit assessment of relative myocardial blood volume (26). Drugs and genetic material could be delivered to tissue by way of microbubbles that could then be destroyed with ultrasound at the required site, providing a means of efficient local delivery.

**Conclusions.** Ultrasound results in microbubble destruction that is more evident at lower frequencies and higher acoustic powers. Reducing the exposure of microbubbles to ultrasound minimizes their destruction. This effect is greater with harmonic than with fundamental imaging with the ultrasound system we used. It is also more pronounced in vivo when microbubbles are injected intravenously than with aortic or direct coronary artery injections. These findings could lead to effective strategies for myocardial perfusion imaging and quantification of myocardial blood flow with venous injections of microbubbles. They could also lead to use of microbubbles for local tissue delivery of drugs and other material.

We are very indebted to Patrick Rafter, MS of Hewlett-Packard Corp. for invaluable engineering assistance, and we thank him for his participation in the in vitro experiments of this study. We also thank N. Craig Goodman, BS for participating in the in vivo experiments.

## References

1. Porter TR, Xie F. Transient myocardial contrast after initial exposure to diagnostic ultrasound pressures with minute doses of intravenously injected microbubbles: demonstration and potential mechanisms. Circulation 1995; 92:2391–5.
2. Burns PN, Powers JE, Simpson DH, Uhlendorf V, Fritzsche T. Harmonic imaging: principles and preliminary results. Clin Radiol 1996;51 Suppl I:50–5.
3. Schrope B, Newhouse VL, Uhlendorf V. Simulated capillary blood flow measurement using a non-linear ultrasonic contrast agent. Ultrason Imaging 1992;14:134–58.
4. de Jong N. Acoustic Properties of Ultrasound Contrast Agents. Woerden (The Netherlands): Zuidam and Zonen, 1993:11.

5. Skyba DM, Camarano G, Goodman NC, Price RJ, Skalak TC, Kaul S. Hemodynamic characteristics, myocardial kinetics and microvascular rheology of FS-069, a second-generation echocardiographic contrast agent capable of producing myocardial opacification from a venous injection. J Am Coll Cardiol 1996;28:1292–300.
6. Gear AR. Continuous flow, resistive particle counting. Anal Biochem 1976; 72:332–45.
7. Jayaweera AR, Edwards N, Glasheen WP, Villanueva FS, Abbott RD, Kaul S. In vivo myocardial kinetics of air-filled albumin microbubbles during myocardial contrast echocardiography: comparison with radiolabelled red blood cells. Circ Res 1994;74:1157–65.
8. Vuille C, Nidorf M, Morrissey RL, Newell JB, Weyman AE, Picard MH. Effect of static pressure on the disappearance rate of specific echocardiographic contrast agents. J Am Soc Echocardiogr 1994;7:347–54.
9. Jayaweera AR, Matthew TL, Sklenar J, Spotnitz WD, Watson DD, Kaul S. Method for the quantitation of myocardial perfusion during myocardial contrast echocardiography. J Am Soc Echocardiogr 1990;3:91–8.
10. Crum LA, Roy RA, Apfel RE, Holland CK, Madanshetty SI. Acoustic cavitation produced by microsecond pulses of ultrasound: a discussion of some selected results. J Acoust Soc Am 1992;91:1113–9.
11. Holt RG, Crum LA. Acoustically forced oscillations of airbubbles in water: experimental results. J Acoust Soc Am 1992;91:1924–32.
12. Roy RA, Church CC, Calabrese A. Cavitation produced by short pulses of ultrasound. In: Hamilton AF, Blackstock DT, editors. Frontiers of Nonlinear Acoustics: Proceedings of 12th International Symposium of Nonlinear Acoustics. London: Elsevier, 1990:476–81.
13. de Jong N, Ten Cate FJ, Lancée CT, Roelandt JRTC, Bom N. Principles and recent developments in ultrasound contrast agents. Ultrasonics 1991;29:324–30.
14. de Jong N. Basic principles of ultrasound contrast agents. In: de Jong N, editor. Acoustic Properties of Ultrasound Contrast Agents, Woerden (The Netherlands): Zuidam and Zonen, 1993:52.
15. Keller MW, Segal SS, Kaul S, Duling BR. The behavior of sonicated albumin microbubbles in the microcirculation: a basis for their use during myocardial contrast echocardiography. Circ Res 1989;65:458–67.
16. Mulvaugh SL, Foley DA, Aeschbacher BC, Klarich KK, Seward JB. Second harmonic imaging of an intravenously administered echocardiographic contrast agent: visualization of coronary arteries and measurement of coronary blood flow reserve. J Am Coll Cardiol 1996;27:1519–25.
17. Kaul S, Kelly P, Oliner JD, Glasheen WP, Keller MW, Watson DD. Assessment of regional myocardial blood flow with myocardial contrast two-dimensional echocardiography. J Am Coll Cardiol 1989;13:468–82.
18. de Jong N. Acoustic properties of ultrasound contrast agents. Woerden (The Netherlands): Zuidam and Zonen, 1993:86.
19. de Jong N. Acoustic properties of ultrasound contrast agents. Woerden (The Netherlands): Zuidam and Zonen, 1993:47.
20. Vandenberg B, Melton HE. Acoustic lability of albumin microspheres. J Am Soc Echocardiogr 1994;7:582–9.
21. Shapiro JR, Reisner SA, Lichtenberg GS, Meltzer RS. Intravenous contrast echocardiography with use of sonicated albumin in humans: systolic disappearance of left ventricular contrast after transpulmonary transmission. J Am Coll Cardiol 1990;1603–7.
22. Singh AK, Behari J. Ultrasound nonlinearity parameters (B/A) in biologic tissues. Indian J Exp Biol 1994;32:281–3.
23. Ungeldorf V. Characteristics of hollow microspheres and their future applications. Proceedings of the First European Symposium on Ultrasound Contrast Imaging, Rotterdam, January 25–26, 1996.
24. Schneider M, Ardifi M, Barrau M, et al. BR-1: a new ultrasonographic contrast agent based on sulfur hexafluoride-filled microbubbles. Invest Radiol 1995;30:451–7.
25. Wei K, Firoozan S, Ates G, Linka A, Goodman N, Kaul S. Quantification of the severity of coronary stenoses using venous injection of minute amounts of AF0180 during intermittent harmonic imaging [abstract]. J Am Coll Cardiol 1997;29 Suppl A:222A.
26. Wei K, Firoozan S, Jayaweera AR, Skyba DM, Goodman NC, Kaul S. Use of microbubble destruction as a novel approach for quantification of myocardial perfusion with contrast echocardiography during venous infusion of contrast [abstract]. J Am Coll Cardiol 1997;29 Suppl A:2A.